



Research Paper / Makale

Iron(III) Complexes Derived From Azo-Containing Salicylaldehyde Ligands: Synthesis, Structures and Biological Evaluations

Kerim SERBEST^{a,*}, Bayram DURAL^b, Melek ÇOL AYVAZ^c, Ali ZENGİN^d, Mustafa EMİRİK^e

^{a,b,c}Department of Chemistry, Recep Tayyip Erdogan University, Rize, Turkey
^cOrdu University, Faculty of Arts and Science, Department of Chemistry, Ordu, Turkey
^dPazar Vocational School, Recep Tayyip Erdogan University, Rize, Turkey
kerimserbest@erdogan.edu.tr

Received/Geliş: 29.03.2021

Accepted/Kabul: 09.06.2021

Abstract: Two novel mononuclear Fe(III) complexes derived from azo-containing salicylaldehyde ligands were synthesized and characterized by elemental analyses, spectroscopic data i.e. IR, ¹H NMR, UV-Vis, electrospray ionization mass spectra, molar conductivity, and magnetic susceptibility measurements. Both the experimental and theoretical results strongly suggest that the ligands have a major contribution to the azo enol imine form instead of the hydrazo keto imine and azo keto amine forms in solution/solid-state. The electronic spectra of the ligands and their iron(III) complexes were calculated theoretically for the band assignments by using DFT and TD-DFT/CPCM methods. DNA binding, cleavage, and antioxidative activities of the investigated compounds were studied. It has been shown that the ligands and their iron (III) complexes tested bind to DNA via the intercalative mode. It was observed that all molecules tested inhibited topoisomerase I almost to the same degree. One of the most striking results among the antioxidant activity tests is that the hydroxyl radical scavenging activities of the ligands and complexes are higher than the standard antioxidant mannitol.

Keywords: Azo-oxime, Iron(III) complex, DFT, DNA interaction, Antioxidant activity.

Azo Grubu İçeren Salisilaldoksım Ligandlarından Türetilen Demir (III) Kompleksleri: Sentez, Karakterizasyon ve Biyolojik Değerlendirmeler

Öz: Azo grubu taşıyan salisilaldoksım türevi ligandlarından türetilen iki yeni mononükleer Fe (III) kompleksi sentezlendi ve elementel analizler, spektroskopik veriler, yani IR, ¹H NMR, UV-Vis, elektrosprey iyonizasyon kütle spektrumları, molar iletkenlik ve manyetik duyarlılık ölçümleriyle karakterize edildi. Hem deneysel hem de teorik sonuçlar, çözelti / katı halde ligandların hidrazo keto imin ve azo keto amin formları yerine azo enol imin formunun daha büyük bir katkısı olduğunu güçlü bir şekilde göstermektedir. Ligandlar ve bunların demir(III) komplekslerinin elektronik spektrumları deneysel spektrumlardaki bant atamaları için, DFT ve TD-DFT / CPCM yöntemleri kullanılarak teorik olarak hesaplandı. Araştırılan bileşiklerin DNA bağlanması, bölünmesi ve antioksidatif aktiviteleri incelenmiştir. Test edilen ligandların ve bunların demir(III) komplekslerinin interkalasyon yaparak DNA'ya bağlandığı gösterilmiştir. Test edilen bütün moleküllerin topoizomerez I' i aynı derecede inhibe ettiği gözlenmiştir. Antioksidan aktivite testleri arasında en çarpıcı sonuçlardan biri, ligandların ve komplekslerin hidroksil radikal süpürücü aktivitelerinin standart antioksidan mannitole göre daha yüksek olmasıdır.

Anahtar Kelimeler: Azo-oksım, Demir(III) kompleksi, DFT, DNA etkileşimi, Antioksidan aktivitesi

1. Introduction

Transition metal complexes have attracted the attention of researchers thanks to their capability for interactions with nucleic acids [1, 2]. Molecules that can interact with DNA have adverse effects on

How to cite this article

Serbest, K., Dural B., Çol Ayvaz, M., Zengin, A., Emirik, M., "Iron(III) Complexes Derived From Azo-Containing Salicylaldehyde Ligands: Synthesis, Structures and Biological Evaluations" El-Cezerî Journal of Science and Engineering, 2021, 8(3); 1184-1201.

Bu makaleye atıf yapmak için

Serbest, K., Dural B., Çol Ayvaz, M., Zengin, A., Emirik, M., "Azo Grubu İçeren Salisilaldoksım Ligandlarından Türetilen Demir (III) Kompleksleri: Sentez, Karakterizasyon ve Biyolojik Değerlendirmeler" El-Cezerî Fen ve Mühendislik Dergisi 2021, 8(3); 1184-1201.

ORCID ID: *0000-0002-2436-8163, ^b0000-0002-9121-4615, ^c0000-0001-5155-5784, ^d0000-0001-6871-4489, ^e0000-0001-9489-9093

DNA replication and transcription. So, they might affect as antitumor reagents by preventing cell growth and division [3]. Therefore, examination of the DNA binding ability of the transition metal complexes is an important research topic [4,5].

Iron, the most common transition metal ion in the human body, does not cause toxicity thanks to its biological feature [6]. Due to its flexible coordination geometries, oxidation states, rotation states and redox potentials, iron is one of the most preferred metals for artificial nuclease synthesis, and multinuclear and mononuclear iron complexes reported as nuclease mimics are known [7]. Oximes and metal complexes are often preferred in biological applications due to their unique properties [8-13]. Azo compounds have also been reported to have excellent thermal and optical properties, so they are used in many applications, such as indicators, recording material, dyeing textile fiber, the coloring of the materials, dye-sensitized solar cells, medical/biological purposes [14-17]. Metal-drugs containing azo-oxime ligands that are hoped not to show the known side effects of commonly used platinum-containing drugs are being investigated in drug discovery studies as an alternative [18,19].

In the present work, we report the synthesis and characterization of two iron(III) complexes with the two azo-containing salicylaldoxime ligands. These complexes are characterized by IR, UV-Vis, mass spectra, elemental analysis, molar conductance, magnetic moment measurements. DFT and TD-DFT calculations were performed to obtain the structural parameters and spectroscopic properties of the compounds and compare with the experimental data. In addition to the ability of the compounds to bind to and cleavage on DNA, their antioxidant activity based on different methods and also their potential to inhibit the topoisomerase enzyme were investigated.

2. Results and Discussion

2.1. Synthesis

Analytical and physical data of mononuclear Fe(III) complexes (3a and 4a) are presented in the experimental section. The azo-oxime type ligands (3, 4) were synthesized by the condensation of related aldehyde (1 or 2) with hydroxylamine hydrochloride in a 1:1 molar ratio in pyridine (Figure 1). Two deprotonated azo-oxime ligands were coordinated to a single iron(III) center through the NO donor atoms. The mass and elemental analyzes data of Fe(III) complexes compatible with IR, UV-Vis data, magnetic and molar conductance measurements showed that the general formula is $[\text{Fe}(\text{HL}^{1 \text{ or } 2})_2\text{Cl}]$, where $\text{HL}^{1 \text{ or } 2}$ are deprotonated oxime ligands. Proposed structures of the mononuclear complexes are shown in Figure 2. The complexes have low solubility in common organic solvents but high solubility in DMF and DMSO.

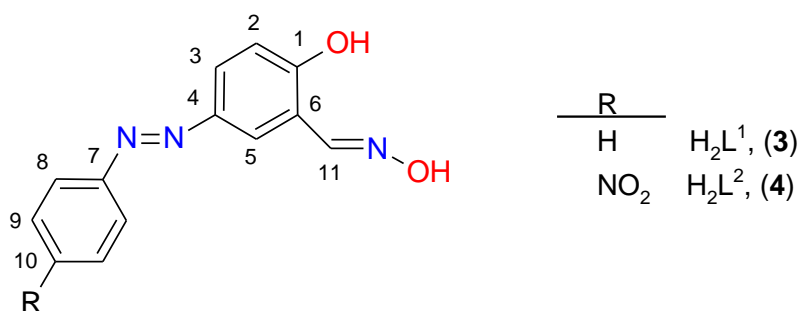


Figure 1. Proposed structure of the ligands.

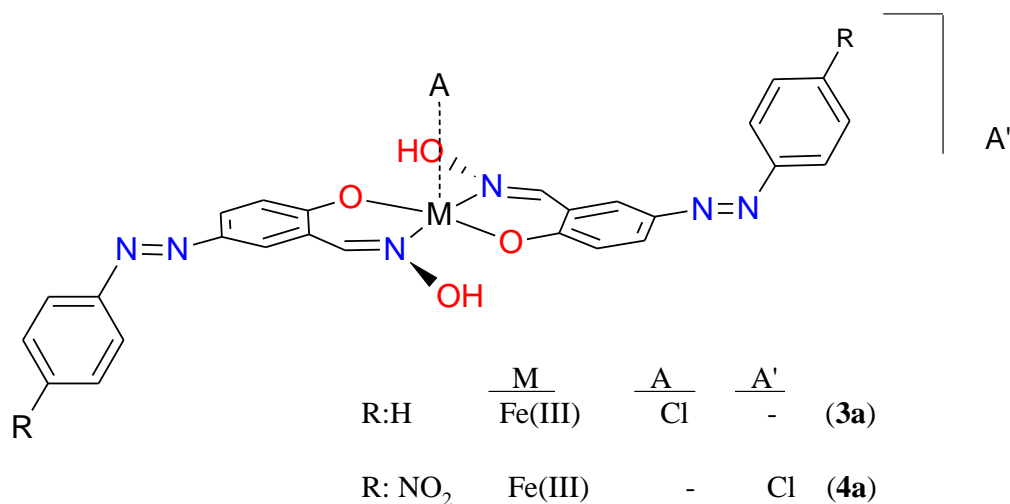


Figure 2. The proposed structures of the mononuclear iron(III) complexes.

2.2. Spectroscopy and DFT Calculations

Vibrational analysis presents useful information to explain the chelating ability of the ligands to Fe(III) ion and some important vibrations of the functional groups in the compounds were given in the experimental section.

The IR spectra of the ligands (H_2L^1 and H_2L^2) show $\nu(\text{C}=\text{N})$ and $\nu(\text{N}-\text{OH})$ peaks at 1633, 3404, and 1603, 3361 cm^{-1} , respectively. In principle, the ligands can exhibit hydrazo keto imine/azo enol imine/azo keto amine tautomerism, since it contains $-\text{N}=\text{N}-$, $\text{H}-\text{C}=\text{N}$, and $-\text{C}-\text{OH}$ functional groups. The only presence of $\nu(\text{O}-\text{H})$ band between 3100 and 3500 cm^{-1} and the missing band $\nu(\text{C}=\text{O})$ approximately at 1700 cm^{-1} indicates that the ligand remains in its azo enol imine form in solid-state. Tautomerism in the present dyes can be illustrated as in Fig. 3. DFT calculations show that the azo enol imine form is more stable than the other tautomeric forms according to relative energies. Optimized geometries of the tautomeric forms and relative energies in the gas phase, chloroform, and DMF solutions were given in Supplementary Fig. S1 and Table S1.

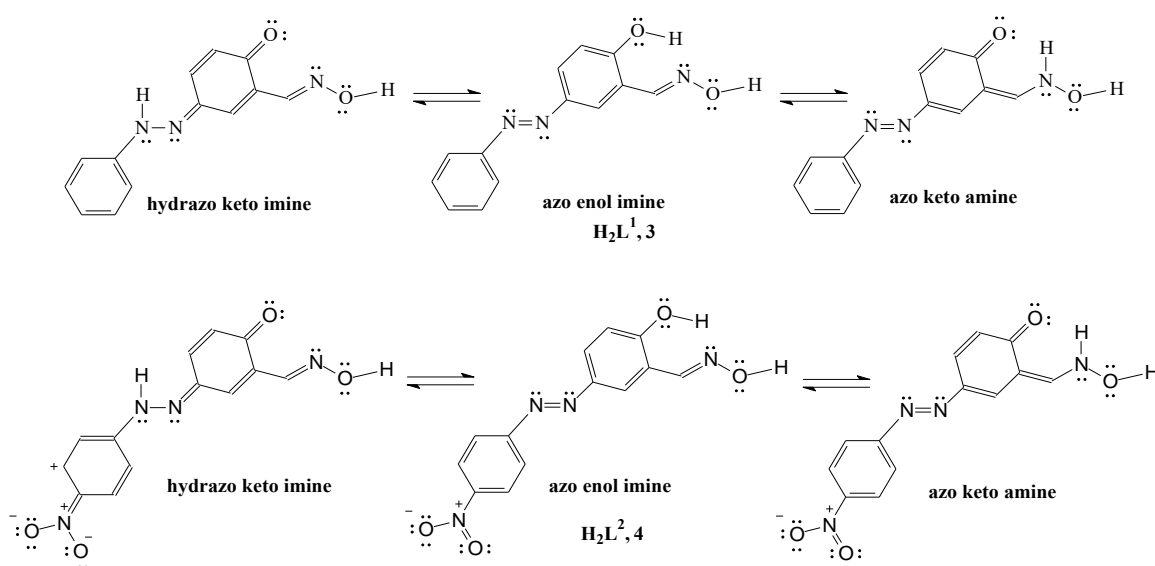


Figure 3. Probable structural configurations of H_2L^1 , (3) and H_2L^2 , (4).

The iron(III) complexes (3a, 4a) show $\nu(\text{C}=\text{N})$ bands at 1592 and 1587 cm^{-1} [20], and it is found that the $\nu(\text{C}=\text{N})$ bands in the complexes are shifted by about 41 and 16 cm^{-1} , respectively, to the higher energy regions compared to the free ligands. This phenomenon appears to be due to the coordination of the azomethine nitrogens to the metal ion [21]. Also, both ligand molecules deprotonated, and thus phenolic OH vibrations at about 3100-3200 cm^{-1} disappear due to the complexation.

Because the vibrations of the bonds containing heavy atoms such as M-N and M-O stretchings fall in the far-IR region, it is difficult to assign vibrations in this region and some tentative assignments were made. In the IR spectra of the complexes, new bands observed in the region 526-418 cm^{-1} (at 423, 523 cm^{-1} for 3a; 418, 526 cm^{-1} for 4a) supported the metal-ligand bonding and assigned to M-N and M-O stretching vibrations, respectively [22]. All the above observations, comparisons, and assignments made from the FT-IR spectra of the ligands and their complexes strongly authenticate the formation of oxime type ligands, (H_2L^1 and H_2L^2) and the complexes, 3a and 4a.

The ^1H NMR spectra of the ligands (H_2L^1 and H_2L^2) in DMSO-d_6 are presented in the experimental section. The singlets at δ 10.333 and 10.378 ppm, respectively, belonging to aldehyde proton of 1 and 2 disappear after the reaction of hydroxylamine hydrochloride with the related aldehyde and two new singlets at δ 8.393 and 8.384 ppm, respectively corresponds to the imine proton resonance (Fig. S2). ^1H NMR spectrum of the ligands clearly demonstrates the presence of a $\text{C}=\text{N}-\text{OH}$ environment. The singlet at δ 11.604 and 11.552 ppm, respectively corresponds to the $\text{C}=\text{N}-\text{OH}$ proton resonance, respectively. The singlets due to $\text{C}=\text{N}-\text{OH}$ at δ 11.604 and 11.552 ppm disappear on deuterium exchange.

The mass spectral studies for the ligands (H_2L^1 and H_2L^2) and their iron(III) complexes were investigated and obtained data are given in the Experimental Section. The mass spectrum of the ligands (H_2L^1 and H_2L^2) exhibit protonated molecular ion at m/z 242 (40.2%) $[\text{M}+\text{H}]^+$ and molecular ion at m/z 287 (100%) $[\text{M}]^+$, respectively which indicates the formation of azo functionalized oxime type ligands (Fig. S3). Analysis by ESI mass spectral data of 3a derived from H_2L^1 indicated ions at m/z 519 (3.4%) $[\text{M}+\text{H}-\text{H}_2\text{O}]^+$. Analysis by ESI mass spectral data of 4a derived from H_2L^2 indicated ions at m/z 750 (16.4%) $[\text{M}+3\text{CH}_3\text{CN}-\text{Cl}]^+$. All these mass spectral data support the formation of the oxime type ligands and their mononuclear iron(III) complexes. The mass spectra of the ligands and their complexes show the molecular ion and corresponding fragmentation peaks.

The electronic spectra of the ligands and their complexes are calculated theoretically for the band assignment. The energies and components of frontier molecular orbitals are important to predict the chemical properties. The orbital energies and some selected frontier orbitals of compounds are given in Fig S4.

The highest occupied molecular orbitals, HOMO, and the lowest unoccupied molecular orbitals, LUMO, of free ligands 3 and 4 are mainly contributed π^* system of the ligands.

The optimized geometries of the Fe(III) complexes (3a and 4a) were shown in Figure 4. The lowest unoccupied molecular orbital of complexes 3a and 4a are the β -LUMO with orbital energy of -4.122 eV and -5.333 eV, respectively. Analysis of the frontier molecular orbital components of the complexes shows that the Fe(III) centers have major contributions to the β -LUMO, β -L+1, β -L+2, β -L+3 orbitals indicating that metal centers behave as an electron acceptor. The highest singly occupied molecular orbitals are the β -HOMO with orbital energies -6.275 eV and -6.571 for 3a and 4a, respectively.

HOMO-LUMO gap indicates the molecular chemical stability and the intensity of electron affinity,

and a lower gap suggests higher electron affinity and chemical reactivity. The molecular orbital energy gaps of the ligands (3 and 4) are decreasing from 6.015 and 5.412 to 2.153 and 1.238 in the related complex structures, respectively. Therefore, the complexes are less stable and more reactive than free ligands. On the other hand, the complex 4a is more reactive than the complex 3a with a lower HOMO-LUMO energy gap. The $-\text{NO}_2$ moiety for 4 and 4a is caused by the lower HOMO-LUMO gap.

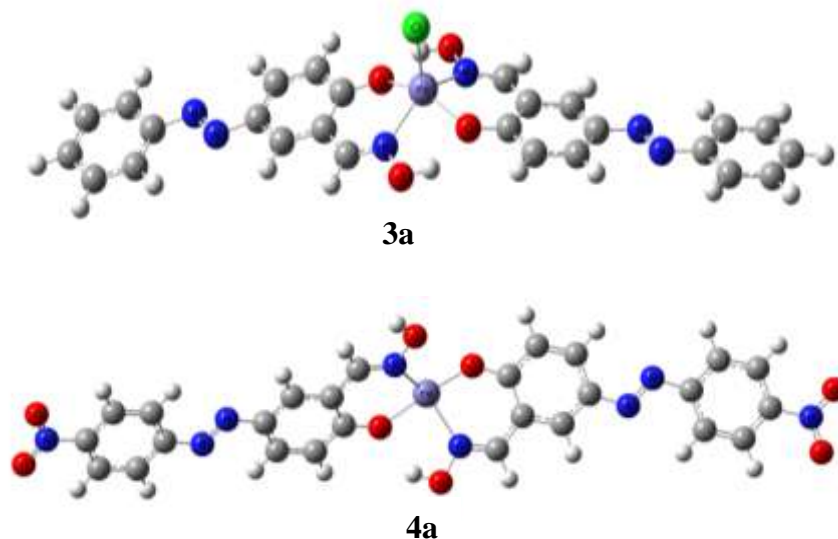


Figure 4. Optimum geometries of 3a and 4a.

The electronic transitions of all of the studied compounds in DMF have been assigned by TDDFT calculations. The experimental absorption bands calculated excited states with major contributions, oscillator strengths, and their assignments are given in Table 1. The highest oscillator strength of electronic transitions which resulted from HOMO to LUMO transitions for the ligands (3 and 4) were obtained at 344 and 374 nm, respectively. Since HOMO and LUMO are mainly composed of π system of the ligands, the bands that appeared experimentally at 359 nm for 3 and 387 nm for 4 were assigned as $L(\pi) \rightarrow L(\pi^*)$ transitions.

The electronic spectrum of 3a showed a weak absorption band at 519 nm which is mainly attributed to $\text{HOMO}(\text{B}) \rightarrow \text{L}+4(\text{B})$ and $\text{H}-1(\text{B}) \rightarrow \text{L}+3(\text{B})$ transitions. This transition can be interpreted as LMCT according to orbital characters. The other two broad bands at 356 and 315 nm mainly result from $\text{H}-1(\text{B}) \rightarrow \text{L}+5(\text{B})$ and $\text{HOMO}(\text{B}) \rightarrow \text{L}+8(\text{B})$ transitions which are assignable to intra ligand charge transfer transitions (ILCT) such as $L(\pi) \rightarrow L(\pi^*)$.

The weak band observed at 872 nm for the complex 4a is mainly caused by $\text{H}-1(\text{B}) \rightarrow \text{L}+3(\text{B})$, $\text{LUMO}(\text{B})$ transitions assigned to d-d transitions. The band centered at 609 nm resulting from the overlap of several transitions, $\text{HOMO}(\text{B})$, $\text{H}-5(\text{B})$, and $\text{H}-6(\text{B})$ which has a larger contribution of donor atoms of the ligand to $\text{LUMO}(\text{B})$, $\text{L}+1(\text{B})$, and $\text{L}+2(\text{B})$ which are mainly metal in character, thus this band is assigned to ligand-to-metal charge transfer (LMCT) transitions. The other observed bands at 417, 364, 358, and 331 nm are assigned as intra-ligand charge transfer ($\pi \rightarrow \pi^*$, $n \rightarrow \pi^*$) based on orbital characters. The TD-DFT/PCM calculations well reproduce the experimentally observed absorption spectrum in DMF solvent.

The magnetic moment of 3a is μ_{eff} 4.58 B.M. ($S = 3/2$). That the coordination number of 3a became five by the axial bonding of chloride caused a significant decrease in magnetic moment value for the d^5 system.

Table 1. Electronic transitions of compounds in DMF.

Comp.	Exp.WL, λ (nm)	Calc.WL, λ (nm)	Osc. Str.	Major contribution	Character	
3	359	344.43	0.9508	HOMO→LUMO (95%)	$n \rightarrow \pi^*$ $\pi \rightarrow \pi^*$	
	334	287.49	0.12	H-2→LUMO (15%), HOMO→L+1 (65%)		
	313	266.64	0.5128	H-2→LUMO (64%), HOMO→L+1 (17%)		
	296	241.44	0.1138	H-4→LUMO (80%)		
		225.76	0.0914	H-2→LUMO (11%), H-2→L+1 (57%), HOMO→L+3 (12%)		
3a	609	645.34	0.026	HOMO(B)→L+5(B) (27%), HOMO(A)→L+1(A) (23%)	LMCT ($n \rightarrow \pi^*$), $\pi \rightarrow \pi^*$	
		595.62	0.049	H-1(B)→L+6(B) (57%)		
		539.95	0.031	H-6(B)→LUMO(B) (49%), H-8(B)→LUMO(B) (19%)		
		529.23	0.058	H-6(B)→LUMO(B) (32%), H-4(B)→L+1(B) (22%)		
		517.63	0.059	H-4(B)→L+1(B) (43%), H-9(B)→LUMO(B) (27%)		
		496.63	0.097	H-5(B)→L+1(B) (71%), H-4(B)→L+2(B) (10%)		
		478.72	0.937	H-5(B)→L+2(B) (16%), HOMO(B)→L+4(B) (33%)		
		417	464.06	0.423		HOMO(B)→L+5(B) (31%), HOMO(A)→L+1(A) (25%)
			458.55	0.013		HOMO(A)→LUMO(A) (84%)
		364	439.16	0.082		HOMO(B)→L+6(B) (28%)
			430.84	0.033		H-4(B)→L+3(B) (55%), HOMO(B)→L+6(B) (10%)
		358	425.56	0.274		H-1(B)→L+4(B) (28%), H-1(A)→LUMO(A) (16%)
			419.42	0.063		HOMO(B)→L+6(B) (30%), HOMO(B)→L+8(B) (16%)
		331	410.61	0.057		H-5(B)→L+3(B) (36%), H-1(B)→L+5(B) (16%)
			367.80	0.013		H-8(A)→L+1(A) (11%), H-1(B)→L+5(B) (15%)
			362.35	0.052		H-5(B)→L+4(B) (28%), H-5(A)→LUMO(A) (23%)
			353.44	0.014		H-19(A)→L+1(A) (14%)
	346.01	0.033	H-7(A)→LUMO(A) (42%), H-7(B)→L+4(B) (44%)			
	335.30	0.032	H-8(B)→L+3(B) (29%), HOMO(B)→L+8(B) (11%)			
4	387	374.13	1.187	HOMO→LUMO (84%)	$n \rightarrow \pi^*$ $\pi \rightarrow \pi^*$	
		302	289.55	0.028		H-3→LUMO (88%)
		269	280.42	0.301		HOMO→L+1 (43%), H-1→LUMO (21%)
			259.23	0.272		HOMO→L+2 (48%), HOMO→L+1 (11%)
			249.05	0.031		H-4→LUMO (55%), HOMO→L+1 (21%)
			232.19	0.134		H-1→L+2 (44%), H-1→LUMO (14%)
4a	872	879.00	0.337	H-1(B)→L+3(B) (35%), HOMO(B)→L+2(B) (55%)	d-d LMCT ($n \rightarrow \pi^*$) $\pi \rightarrow \pi^*$	
		801.55	0.003	H-1(B)→L+3(B) (51%), HOMO(B)→L+2(B) (38%)		
		699.05	0.018	H-1(B)→L+2(B) (49%), HOMO(B)→L+3(B) (36%)		
		519	590.26	0.013		HOMO(A)→LUMO(A) (21%), HOMO(B)→L+4(B) (24%)
			505.15	0.039		
			501.69	0.003		HOMO(B)→L+4(B) (48%), HOMO(B)→L+6(B) (18%)
			497.65	0.127		H-4(B)→L+1(B) (80%)
			460.36	0.046		H-5(B)→L+1(B) (76%)
			404.95	0.059		H-5(B)→L+3(B) (78%)
			401.53	0.858		H-8(B)→L+2(B) (49%), H-6(B)→L+2(B) (17%)
		356	395.75	0.024		H-12(B)→LUMO(B) (34%), HOMO(B)→L+6(B) (13%)
			379.18	0.209		H-11(B)→LUMO(B) (33%), H-6(B)→L+2(B) (25%)
		315	377.91	0.448		H-11(B)→L+2(B) (18%), H-7(B)→L+3(B) (33%)
			375.12	0.111		HOMO(A)→LUMO(A) (14%), H-11(B)→L+2(B) (32%)
			369.75	0.041		H-1(A)→L+1(A) (55%), HOMO(A)→LUMO(A) (31%)
			361.59	0.037		H-11(B)→L+2(B) (11%), H-10(B)→L+2(B) (44%)
			354.20	0.033		H-1(B)→L+5(B) (39%), HOMO(B)→L+6(B) (24%)
			347.24	0.136		H-1(B)→L+5(B) (14%)
			331.74	0.019		H-15(B)→L+3(B) (42%), HOMO(B)→L+8(B) (14%)
	326.83	0.122	H-1(A)→L+3(A) (27%)			
	309.05	0.012	H-4(B)→L+6(B) (13%), HOMO(B)→L+8(B) (18%)			
			H-6(A)→LUMO(A) (17%), H-6(B)→L+4(B) (36%)			

The decrease could be assignable to the distorted square pyramidal geometry around Fe(III) in the structure of 3a. The magnetic moment of 4a has μ_{eff} 5.12 ($S = 5/2$) B.M. and this observed value indicates distorted tetrahedral geometry around the Fe(III) ion [23].

Molar conductance values of the iron(III) complexes (3a, 4a) were taken from 10^{-3} M DMF solutions at 20 ± 2 °C and the obtained values of the complexes were given in the experimental section. Complex 3a has a very small conductance, indicating that it is non-electrolyte while 4a is found to have a molar conductance value of $85 \Omega^{-1} \text{ mol}^{-1} \text{ cm}^2$ indicating uncoordination of the chloride to Fe(III) ion [24]. This value showed obviously that 4a is ionic in nature and 1:1 type electrolyte.

2.3. DNA Binding Studies

Firstly, the DNA binding abilities of the studied molecules were searched by using electronic absorption spectroscopy. Absorption titration studies were carried out by adding calf thymus DNA (CT-DNA) in varying proportions (0-38 μM) to the complex solution of constant concentration (1.5×10^{-5} M) in Tris-HCl/NaCl buffer and monitoring the absorption spectrum after a 10 minutes incubation after each addition.

The absorption spectra for the ligand, 3, 4, and their iron(III) complex, 3a, 4a are shown in Figure 5.

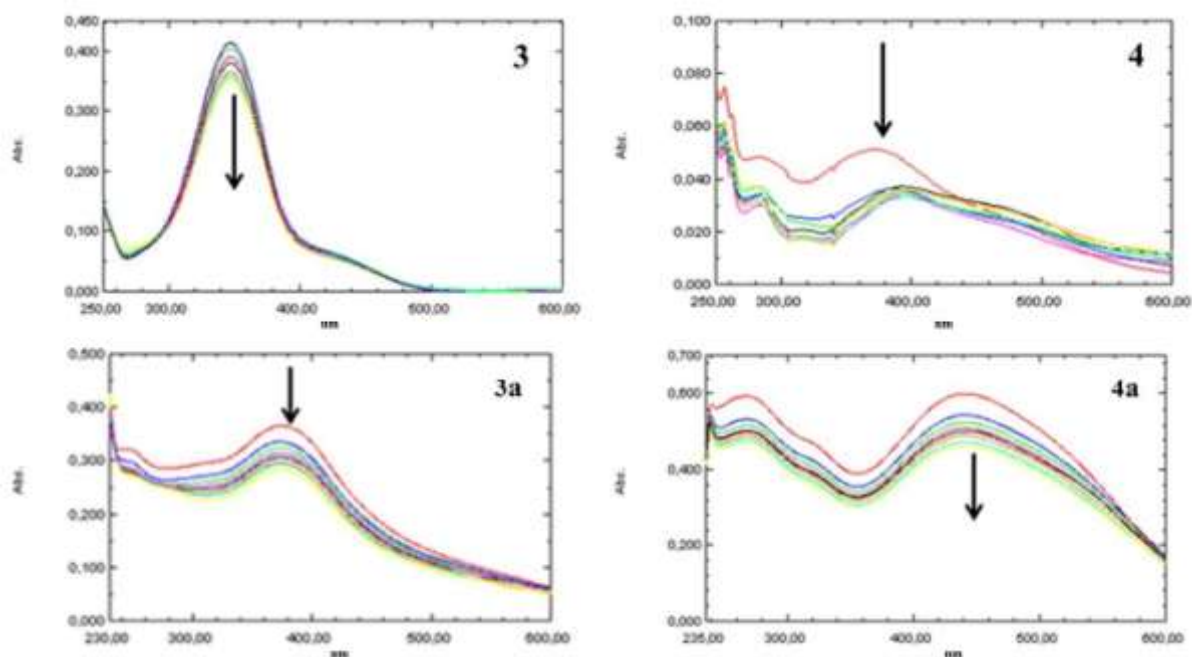


Figure 5. Absorption spectra of the H_2L^1 (3), H_2L^2 (4) and their mononuclear Fe(III) complexes (3a and 4a) (1.5×10^{-5} M) The arrow shows the absorbance changing upon increasing the DNA concentrations (0-38 μM).

As can be seen from Figure 5, with the addition of DNA, the absorption density of complexes (3a, 4a) and ligand (3, 4) decreases gradually, and absorption spectra with similar profiles were obtained for all. When the absorption spectrum obtained for the ligand (3) is examined in detail, it is seen that 15% hypochromite around 347 nm is accompanied by a very small 0.5 nm redshift. In the case of ligand 4, both the severity of the redshift (25 nm) and the hypochromite (%29) are higher. In the presence of complexes (3a and 4a), the direction of the shifts is blue, but the degree of shift and hypochromite intensity is almost the same.

Briefly, when CT-DNA was added to all studied molecules, different rates of decrease in maximum absorbance (hypochromism) and shift in wavelength in varying rates and directions were observed. These observations indicate that all molecules are intercalated to CT-DNA as evidence of intercalation. Since the strength of the molecule's binding to DNA can be correlated with the size of the spectral change, it can be interpreted that the DNA binding activity in both complexes (3a and 4a) is almost the same. Moreover, binding constants of the ligands and the complexes were calculated and found as 1.0×10^4 and 1.0×10^5 , respectively.

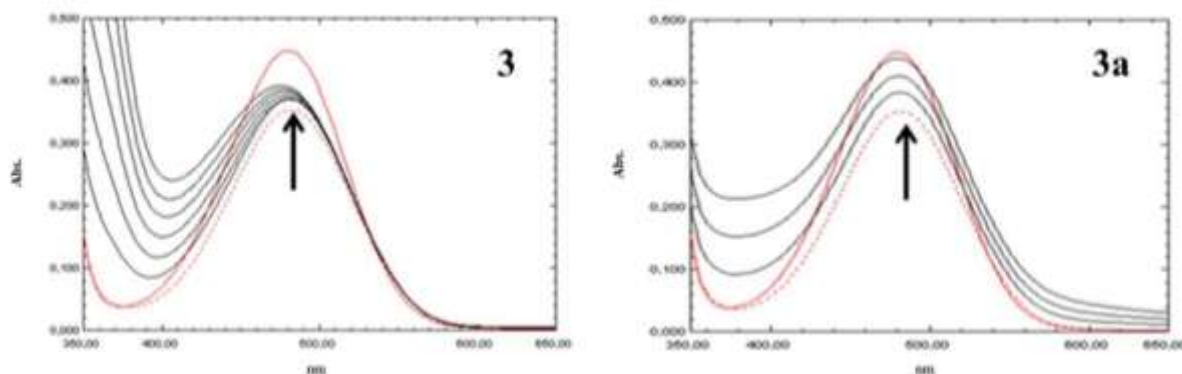


Figure 6. Absorption spectra of EB bound to DNA in the absence and presence of the increasing amount of **3** (5, 10, 15, 20, 25, 30 μM) and **3a** (2.5, 5.0, 7.5 μM). (—): 40 μM EB, (.....):40 μM EB + 40 μM CT-DNA, (—):40 μM EB + 40 μM CT-DNA + **3/3a**. Arrow (\uparrow) is in the direction of the absorbance change with increasing concentrations of **3** and **3a**.

Competitive ethidium bromide (EB) binding study was carried out using absorption spectroscopy technique to show whether the molecules examined will bind to DNA instead of EB, which is known to bind to DNA by intercalation [25]. When EB is intercalated between DNA base pairs, the maximum absorption of free EB around 480 nm shifts to a higher wavelength, and a decrease in absorption is exhibited as evidence of intercalation [26]. It can be seen from Figure 6 that the absorption maximum of free EB (480 nm) is shifted to 482 nm as expected in the presence of DNA. With increasing amounts of **3** and/or **3a** added to the EB-DNA solution, a progressive increase in absorption density is observed, indicating that the tested molecules compete with EB in order to bind to DNA. Similar profiles were found in cases **4** and **4a**. These absorption spectrum profiles obtained are another indication that all of the molecules tested are bound to DNA by intercalation mode.

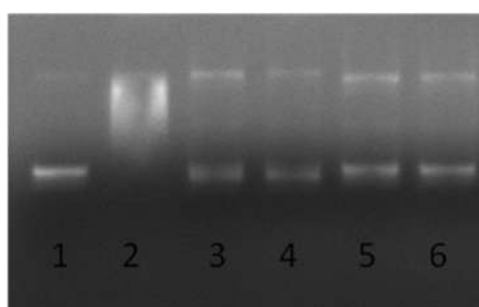


Figure 7: Electrophoretic representation of the inhibition of topoisomerase I enzyme in the presence of ligands and complexes. 1: DNA (250 ng), 2: DNA+ Human Topo I (0.3 U), 3-6: DNA + Human Topo I + **4, 3, 4a, 3a** (0.4 mM).

Topoisomerase I, an enzyme that contributes to the process by helping to open the DNA helix during transcription or replication, is one of the cellular targets in anticancer therapy [27, 28]. DNA intercalators can inhibit the functions of topoisomerases by filling the binding site of topoisomerase

on the DNA or forming stable ternary complexes [28]. Effects on the topoisomerase activity of Azo-oxime ligands and their Fe(III) complexes, which are expected to bind to DNA by intercalation by other tests, were also investigated.

It can be seen from Figure 7 that the complete relaxation of the supercoiled pBR322 by the effect of Topoisomerase I was prevented by the addition of 0.4 mM molecule. It is observed that all molecules inhibit topoisomerase I moderately, preventing DNA relaxation.

2.4. DNA Cleavage Studies

2.4.1. Hydrolytic DNA Cleavage

The hydrolytic cleavage activities have been performed by changing several factors such as medium pH, ligand/complex concentration, ionic strength, and incubation time using supercoiled plasmid pBR322 DNA. To determine the effect of pH on hydrolytic DNA cleavage, the reaction mixtures were prepared using buffers with different pH values. To establish the dependency on concentration of DNA cleavage activity of the ligands and complexes, pBR322 DNA were incubated with different concentrations of the molecules in Tris-HCl buffer at pH value determined as optimum, for 6 h. An ionic strength study was performed to test the electrostatic contribution to DNA cleavage by the addition of a strong electrolyte, such as NaCl. In this experiment, except for the addition of NaCl at different concentrations, molecule concentration and the medium pH were kept constant according to values determined by means of previous experiments. Investigation of the time dependence of the molecules for DNA hydrolysis was performed by using the effective values obtained for pH, molecule, and NaCl concentrations. Except for these, the constant DNA concentration was used for each sample. Samples were incubated for different periods (1, 3, 6, and 12 h).

As can be seen from Figure , 3 and 3a were the most effective in terms of DNA cleavage at pH 6 and pH 5 when using Tris-HCl buffer. When phosphate buffer was preferred for the same pH value, the activity was very less. Zhu explained this situation as follows: the binding site of the metal complex was the negatively charged phosphates of the DNA backbone and the competition of the phosphates in pH buffer with the phosphates on the DNA backbone might be inhibited the binding event between molecules and DNA [29].

As the concentration of 3a increases (10-250 μ M), the amount of supercoiled form decreases and the nicked form increases, indicating that the cleavage activity increases. In the case of ligands (3 and 4), unlike complexes, no increase in the nuclease activity was observed even when the concentration was increased to 2mM (image is not shown). Similarly, while the maximum cleavage activity was observed in the presence of 10 μ M 4a, a decrease in the activity occurred when higher concentrations were reached.

According to results of the ionic strength assay, as it can be visible well from the Figure 7C, at low salt concentrations, an increase was firstly observed, then a decline occurred at cleavage profile as salt concentration increases in the presence of constant concentration of 4a. The most effective salt concentration for 4a was 10 mM. Thus, it can be concluded that there is an electrostatic contribution to the DNA cleavage reaction [29].

At the last experiment, with reaction time increases, formation of Form II increased and Form I gradually faded. That is to say, DNA cleavage activity of the studied complexes is dependent on the reaction time.

To speculate a mechanism for DNA cleavage, cleavage experiments were carried out in the presence of some standard radical scavengers [30]. EtOH, MeOH, *t*-BuOH, NaN₃, L-histidine, KI and DMSO used as radical scavenger did not alter the activity (Image is not given). These rules out the possibility of cleavage by hydroxyl radical, singlet oxygen, and hydrogen peroxide.

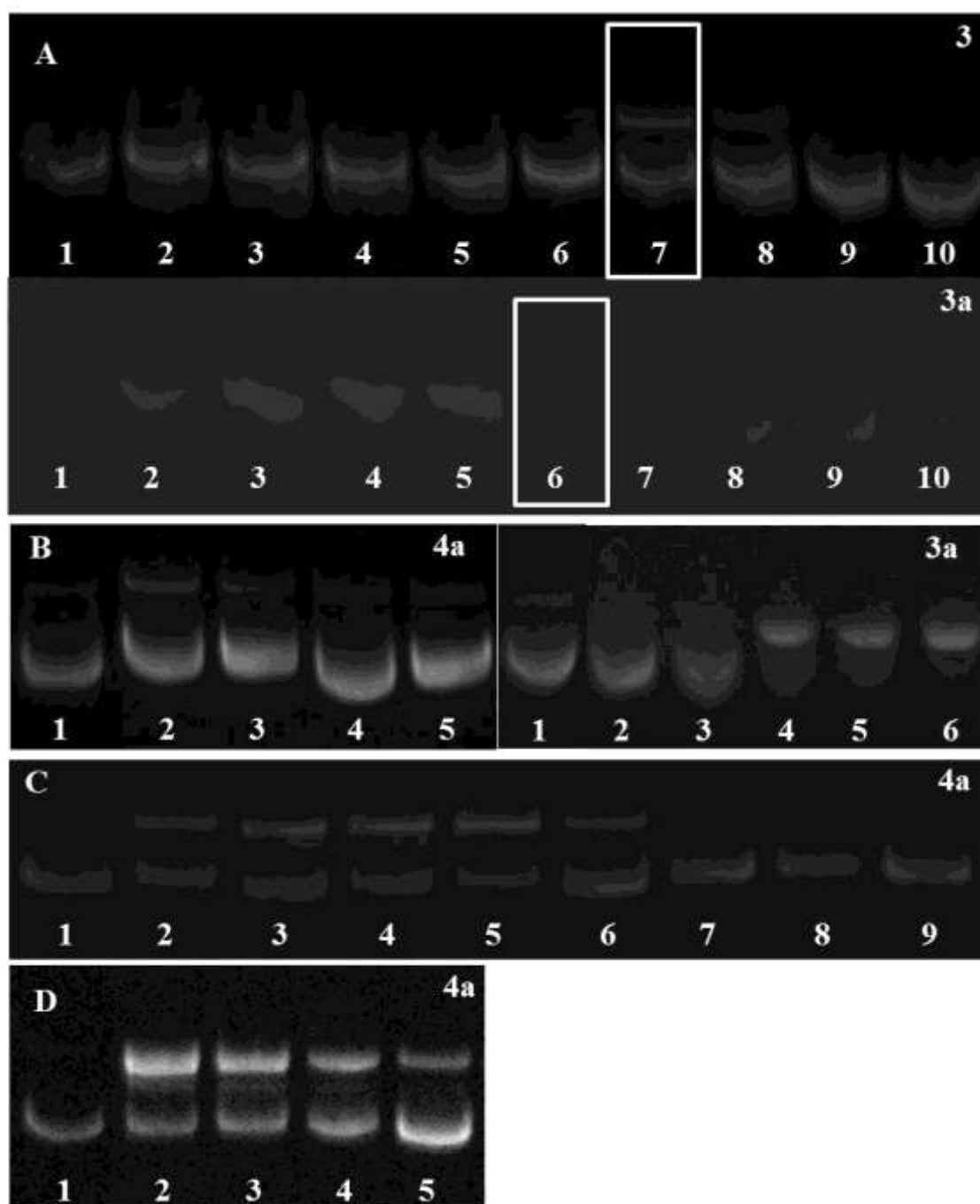


Figure 8. A: pH dependence of the DNA cleavage activity of 3 and 3a. 1: DNA control, 2-5: phosphate (50 mM, NaH₂PO₄-Na₂HPO₄) buffer (pH 6→9) was used; 6-10: 50 mM Tris-HCl buffer (pH 5→9) was used. B: Concentration dependence of the DNA cleavage of 4a and 3a. 1: DNA control. 2-5: 10-50-100-250 μM for 4a; 10-20-50-100-250 μM for 3a. C: Ionic strength dependence of DNA cleavage activity of 4a. 1: DNA control; 2-9: 0-2.5-5-10-50-100-250-350 mM NaCl D: Reaction time dependence of DNA cleavage activity of 4a. 1: DNA control; 2-5: 12, 6, 3 and 1 h.

The SOD enzyme has a distinct influence on the DNA cleavage suggesting that the superoxide anion is involved in the cleavage process. By the way that as a metal chelating agent EDTA binds strongly to the metal in complex structure, forming a stable complex, it is not surprising that the complexes tested significantly inhibit the DNA cutting activity [31]. Because EDTA did not affect the nuclease activity of the ligands.

2.4.2. Oxidative DNA Cleavage

For this assay, reaction mixtures were prepared to contain one of these auxiliary reagents at different concentrations: H_2O_2 (0.4 M), AA (ascorbic acid, 2.5 mM), mercaptoethanol (ME, 0.4 M) and dithiothreitol (DTT, 0.32 mM) as well as 200 ng supercoiled DNA, 25 μM complex/125 μM ligand, and in 50 mM Tris-HCl buffer (pH 7) unlike the hydrolytic cleavage. The incubation period was 3 h at 37 °C. The inductive effects of other tested agents, except for ME, are equivalent in the case of all molecules. ME exhibited a reducing rather than inducing effect. The agarose gel electrophoresis image for 3a (as representative examples) are in Figure . By taking into account the concentrations of the external agents it can be said that the activator effect of the H_2O_2 was lower than others. It can be thought that the increase in the production of hydroxyl radicals with the addition of hydrogen peroxide may lead to an increase in nuclease activity [32]. The inductive effect of the AA was most in the presence of 3a, particularly. As a result of all these experiments, it can be said that 3a and 4a can cleave DNA both through hydrolytic and oxidative patterns.



Figure 9. Nuclease activity of the 3a in the presence of the auxiliary reagents. 1: DNA+ 3a; 2: DNA+3a+ H_2O_2 (0.4 M); 3: DNA+3a+ME (0.4 M); 4: DNA+3a+AA (2.5 mM); 5: DNA+3a+DTT (0.32 mM).

2.5. Antioxidative Activities

Molecules with antioxidant properties could potentially have a crucial role in the elimination of the reactive oxygen species (ROS) which can be produced during normal metabolic processes in the life of aerobic organisms, and repair of damaged DNA. Furthermore, it is a well-known fact that transition metal complexes have significant antioxidative activity [33-35]. From this point of view, we decided to investigate the antioxidative potential of the studied ligands and their iron(III) complexes in terms of DPPH, hydroxyl, and superoxide radicals scavenging activity.

Radical scavenging activities of the ligands and their Fe(III) complexes were calculated as SC_{50} , the concentration scavenging the 50% of the free radicals in the medium, and compared with the results calculated for standard antioxidants.

As can be seen from Table 2, the scavenging activity of the ligands and their Fe(III) complexes on hydroxyl radical is very much higher than the standard mannitol. While a similar situation was available for DPPH free radical scavenging activity values, superoxide dismutase scavenging activities were lower than the commercial SOD enzyme. Another noteworthy point is that the activities of the ligands were lower than their complexes. As a conclusion, investigated Fe(III)

complexes are more effective radical scavenging power compared to standard antioxidants, and their DNA binding and DNA cleavage abilities and antioxidative activities are also much more than ligands.

Table 2. Antioxidative activities of the ligands or complexes expressed as SC_{50} .

Ligands/complexes	SC_{50} (SOD) (μ M)	SC_{50} (DPPH) (μ M)	SC_{50} (HRSA) (μ M)
3	52.5 \pm 2.3	330.76 \pm 11.8	107.86 \pm 3.85
4	175.4 \pm 5.8	74.15 \pm 1.4	6.18 \pm 0.95
3a	33.0 \pm 1.5	1.21 \pm 0.5	2.64 \pm 0.24
4a	54.5 \pm 3.7	15.91 \pm 0.75	4.47 \pm 1.20
SOD	0.025 \pm 0.002	-	-
Ascorbic acid	-	27.05 \pm 1.2	-
BHA	-	147 \pm 5.3	-
Mannitol	-	-	10860 \pm 17.35

3. Experimental

3.2. Physical Measurements

Melting points (m.p.) were determined on a Barnstead/Electrothermal 9100 apparatus in open capillary tubes. The FTIR spectra were measured as KBr pellets on a Perkin-Elmer 100 FTIR spectrometer. ^1H NMR and were recorded on a Varian Gemini 200 and Varian Mercury 400 spectrometer using DMSO- d_6 solvent. Chemical shifts (δ) are reported in part per million (ppm) relative to an internal standard of Me_4Si . The ultraviolet-visible spectra were measured on a Shimadzu 1601-PC UV/Vis spectrophotometer using DMF as the solvent. Room temperature (296 K) solid-state magnetic susceptibility was measured by using a Sherwood Scientific magnetic susceptibility balance. $\text{MnCl}_2 \cdot 6\text{H}_2\text{O}$ was used as the standard. Elemental analyses were determined on a Costech 4010 CHNS instrument. Metal containing of the complexes was determined by Spectro Genesis Optical emission spectrometer with inductively-coupled plasma excitation (ICP) and electrospray ionization mass spectrometry (ESI-MS) was performed on a Thermo Quantum Access Max LC-MS/MS spectrometer at Recep Tayyip Erdoğan University Central Research Laboratory, Rize, Turkey. Solution electrical conductivities were measured at room temperature with approximately 10^{-3} M DMF solutions, with a Hanna EC 215 conductivity meter by using 0.01 M KCl water solution as calibrant.

3.3. Materials

All of the reagents and solvents involved in synthesis were of analytical grade and used as received without further purification. Salicylaldehyde, p-nitroaniline, aniline, hydroxylamine hydrochloride, anhydrous FeCl_3 were purchased from Aldrich and Merck. Azo-coupled salicylaldehyde precursors, 2-Hydroxy-5-[(*E*)-phenyldiazenyl]benzaldehyde (1) and 2-hydroxy -5-[(4- nitrophenyl)diazenyl] benzaldehyde (2) and the parent ligands, 2-hydroxy-5-[(*E*)-(4-phenyl)diazenyl]benzaldehyde oxime, H_2L^1 , (3), 2-hydroxy-5-[(*E*)-(4-nitrophenyl)diazenyl]benzaldehyde oxime, H_2L^2 , (4), were prepared according to the literature [36].

3.4. Computational Details

Density functional calculations were performed by using the Gaussian 09 software package [37].

The hybrid, Becke-3-Lee Yang Parr (B3LYP) density functional theory method [38] with 6-311G++(d, p) triple-zeta basis set with polarization functions [39] for the H, C, N, and O atoms and the Los Alamos effective core potentials plus the Double Zeta (LANL2DZ) [40] basis set for the Fe atom in ground state was used for all theoretical computations. Full optimizations were performed for all compounds with the DFT/B3LYP methods in the gas phase. The relative stability of tautomeric forms of the ligands was also calculated with the same level of theory in the gas phase and selected solvents using a conductor-like polarizable continuum model (CPCM) model. Harmonic frequency analyses indicate that the optimized structures are at stationary points corresponding to local minima with real vibrational spectra. Electronic excitations were calculated using the time-dependent density functional theory (TD-DFT) formalism [41] using CPCM [42]. The lowest 100 singlet-singlet transitions of metal complexes and 60 singlet-singlet transitions of the ligands were computed in the implicit solvent of DMF. GaussSum was used to describe the UV/Vis bands characters [43]. GaussView 5.0 was used to visualize the results of computations [44].

3.5. Synthesis of the Ligands

The ligands were prepared by a general method. The solution of aldehyde precursor (1 or 2) (5 mmol) and excess hydroxylamine hydrochloride (15 mmol) in dry pyridine (100 cm³) was stirred for two days at room temperature and then the reaction mixture was then poured into ice-cold H₂O (~350 cm³). The resulting precipitate was filtered, washed with cold H₂O and petroleum ether several times, and recrystallized from the hot ethylacetate-petroleum ether. The obtained microcrystalline yellow solid was dried in vacuo over CaCl₂ [36, 45].

2-Hydroxy-5-[(E)-(4-phenyl)diazenyl]benzaldehyde oxime, H₂L¹, (3) (yield 94%, color: yellow, m.p.: 155°C)

Anal. Calc. for C₁₃H₁₁N₃O₂: C, 64.72; H, 4.60; N, 17.42. Found: C, 64.66; H, 4.67; N, 17.51%. UV/Vis (DMF) λ_{max} (ϵ): 296 (39810); 313 (38410); 334(33240);359 (39820); 396(30080). IR (cm⁻¹): 3404 ν (N-OH); 1633 ν (C=N); 1481 ν (N=N); 1224 ν (C-O). ¹H NMR (400 MHz, DMSO-d₆) δ : 7.065, 7.043 d. (Ar-1H, J=8.8 Hz); 7.5-7.04 m.(Ar-3H); 7.8-7.78 m.(Ar-3H); 8.082 s. (Ar-1H); 8.393 s. (1H, H-C=N); 11.604 s. (1H, C=N-OH); 10.958 (Ar-OH). MS(ESI-*m/z*): 242 [M]⁺.

2-Hydroxy-5-[(E)-(4-nitrophenyl)diazenyl]benzaldehyde oxime, H₂L², (4) (yield 67%, color: brown, m.p.: 202°C)

Anal. Calc. for C₁₃H₁₀N₄O₄: C, 54.55; H, 3.52; N, 19.57. Found: C, 54.62; H, 3.53; N, 19.53%. UV/Vis (DMF) λ_{max} (ϵ): 269 (12470); 302(13930); 387(18900); 607 (3480). IR (cm⁻¹): 3361 ν (N-OH); 3130 ν (OH); 1603 ν (C=N); 1488 ν (N=N); 1336 ν (NO₂); 1271 ν (C-O). ¹H NMR (200 MHz, DMSO-d₆) δ : 7.062, 7.107 d. (Ar-1H, J=9.0 Hz); 7.855, 7.898 d. (Ar-1H, J=8.6 Hz); 7.961, 8.006 d. (Ar-2H, J=9.0 Hz); 8.172 s. (Ar-1H); 8.166, 8.209 d. (Ar-2H J=8.6 Hz); 8.384 s. (Ar-1H, H-C=N); 11.135 s. (Ar-OH); 11.552 s. (C=N-OH). MS(ESI-*m/z*): 287 [M+H]⁺.

3.6. Preparation of Metal Complexes (3a, 4a)

Complexes 4a was synthesized following the same procedure adopted for 3a.

Chloro bis{(2-Hydroxy-5-[(E)-(4-phenyl)diazenyl]benzaldehyde oximate)}iron(III), (3a): (yield 84%, color: dark green, m.p.: 260 °C).

A solution of FeCl₃ (34 mg; 0.21 mmol) in 5 mL ethanol was added dropwise to the solution of H₂L¹ (100 mg; 0.41 mmol) in 20 mL ethanol and the resulting solution was stirred for two days at

room temperature. The pH of the solution was adjusted to 6.5 with ammonia. Then, the precipitate was formed and the mixture was additionally stirred for 1 h. The microcrystalline green solid product was isolated by filtration and washed with H₂O, finally dried in vacuo over CaCl₂.

Anal. Calc. For C₂₆H₂₀N₆O₄ClFe; C, 54.6; H, 3.5; N, 14.7; Fe, 9.8 Found: C, 54.7; H, 3.6; N, 15.1; Fe, 9.9. UV-Vis (DMF) λ_{max} (ϵ): 274 (10930); 331 (12130); 358(13160); 364 (13180); 417 (13160); 609(26240). IR (cm⁻¹): 3171 ν (N-OH); 1592 ν (C=N); 1463 ν (N=N); 1231 ν (C-O); 523 ν (M-O); 423 ν (M-N). Molar conductivity (Ω^{-1} cm² mol⁻¹) 8. μ_{eff} B.M. (298 K): 5.12 (for per metal ion); MS(ESI-m/z): 519 [M-OH-Cl]⁺.

Bis{2-Hydroxy-5-[(E)-(4-nitrophenyl)diazanyl]benzaldehyde oximato}iron(III) chloride, (4a): (yield 83%, color: dark green, m.p.: 285 °C).

Anal. Calc. For C₂₆H₁₈N₈O₈ClFe; C, 47.2; H, 2.7; N, 16.9; Fe, 8.4 Found: C, 47.5; H, 2.9; N, 17.1; Fe, 8.7. UV-Vis (DMF) λ_{max} (ϵ): 274 (27160); 315 (18240); 356 (8160); 519 (13020); 871 (444). IR (cm⁻¹): 3392 ν (N-OH); 1587 ν (C=N); 1472 ν (N=N); 1338 ν (NO₂); 1205 ν (C-O); 526 ν (M-O); 418 ν (M-N). Molar conductivity (Ω^{-1} cm² mol⁻¹) 85. μ_{eff} B.M. (298 K): 4.58; MS(ESI-m/z): 749 [M+3CH₃CN-2H₂O]⁺.

3.7. Biological Studies

All chemicals used throughout the biological studies were of analytical reagent grade and were provided commercially by Sigma. DNA binding experiments were carried out by using UV-Visible absorption spectrophotometer. Absorption titration studies were carried out maintaining the free ligand or its corresponding metal complex concentration constant (15 μ M) and gradually increasing the concentration of CT-DNA (0-38 μ M) in the 5 mM Tris-HCl/50 mM NaCl buffer solution (pH=7.2). Binding constants were calculated using following equation:

$$[\text{DNA}]/(\epsilon_a - \epsilon_f) = [\text{DNA}]/(\epsilon_b - \epsilon_f) + 1/Kb(\epsilon_b - \epsilon_f) \quad (1)$$

In the equation, [DNA] is the concentration of DNA, ϵ_a is the apparent extinction coefficient (A_{obs}/M), ϵ_b is the extinction coefficient of the free metal and ϵ_f is the the extinction coefficient for the metal complex in the fully bound form [46].

Furthermore, to support the interaction type, the competitive binding experiments were done by using ethidium bromide with the method used by the literature [47]. Topoisomerase inhibition effect was also evaluated by observing the relaxation of supercoiled DNA on an agarose gel according to the reported method [27]. Under different reaction conditions such as pH, concentration, ionic strength, and reaction time, the hydrolytic cleavage efficiency of ligands and complexes on plasmid pBR322 DNA was examined using agarose gel electrophoresis technique. Efficiencies of ROS on hydrolytic cleavage were also searched in the presence of various standard radical scavengers such as DMSO, tert-butyl alcohol, EtOH, MeOH, NaN₃, L-Histidine, SOD, EDTA, catalase and KI [48-50]. Besides, cleavage experiments were carried out in the presence of auxiliary reagents as H₂O₂, ascorbic acid (AA), mercaptoethanol (ME) and dithiothreitol (DTT) to test oxidative cleavage [51]. Antioxidative activities of ligands and their complexes were determined by DPPH free radical [52], hydroxyl radical [53], and superoxide radical [54] scavenging activities.

4. Conclusions

Two novel mononuclear iron(III) complexes (3a, 4a) with azo-containing salicylaldehyde ligands have been synthesized and characterized by physicochemical and spectroscopic methods. The electronic spectra of the ligands and their Fe(III) complexes are calculated theoretically for the band assignment by using DFT and TD-DFT/CPCM methods. Investigated ligands and their iron(III) complexes bind to DNA through an intercalative mode according to results of DNA binding studies. Furthermore, 3a and 4a can cleave DNA both through hydrolytic and oxidative ways. The investigated Fe(III) complexes are more effective radical scavenging power compared to known antioxidants used as standard. Obtained high enough binding constant values and a good level of antioxidant activities are those parameters that are required for the design of new anticancer drugs.

Acknowledgments

The authors thank Recep Tayyip Erdoğan University, Central Research Laboratory (Rize/Turkey) for obtaining mass spectra and determining of metal-containing of compounds. The Scientific and Technological Research Council of Turkey (TUBİTAK) supported this study with a project (Project Number: 112T526).

Authors' Contributions:

Kerim Serbest: Conceptualization, Methodology, Supervision, Writing - review & editing. Bayram Dural: Investigation. Melek Çöl Ayvaz: Writing, Investigation. Ali Zengin: Investigation. Mustafa Emirik: Software.

Competing Interests:

The authors declare that they have no competing interests.

References

- [1]. Ragheb, M. A., Eldesouki, M. A., Mohamed M. S., "DNA binding, photo-induced DNA cleavage and cytotoxicity studies of lomefloxacin and its transition metal complexes", *Spectrochim Acta A Mol Biomol Spectrosc.*, 2015, 138: 585–95. doi: 10.1016/j.saa.2014.11.046
- [2]. Zeng, P., He, L., Ye, Z., Yang, N., Song, Y., Lu, J., "DNA interactions, antitumor activities and radical scavenging properties of oxovanadium complexes with pyrazino[2,3-f][1,10]phenanthroline ligands", *Transit. Met. Chem.*, 2015, 40: 779–787. doi: 10.1007/s11243-015-9939-9
- [3]. Iglesias, B. A., Barata, J. F. B., Pereira, P. M. R., Girão, H., Fernandes, R., Tomé, J. P. C., Neves, M. G. P. M. S., Cavaleiro, J. A. S., "New platinum(II)–bipyridyl corrole complexes: Synthesis, characterization and binding studies with DNA and HSA", *Journal of Inorganic Biochemistry*, 2015, 153: 32-41. doi:http://dx.doi.org/10.1016/j.jinorgbio.2015.08.016
- [4]. Karia, P. S., Vekariya, P. A., Patidar, A. P., Kanthecha, D. N., Bhatt B. S., and Patel, M. N., "DNA Interaction, in vitro Antibacterial and Cytotoxic Activities of Ru(III) Heterochelates", *Acta Chim. Slov.*, 2019, 66: 944–949. doi:10.17344/acsi.2019.5159
- [5]. Kanthecha, D. N., Raval, D. B., Thakkar, V. R., Patel, M. N., "Biological Significance of Hetero-Scaffolds Based Gold(III) Complexes", *Acta Chim. Slov.*, 2018, 65: 333–343. doi:10.17344/acsi.2017.4018
- [6]. Terenzi, A., Barone, G., Silvestri, A., et al., "The interaction of native calf thymus DNA with Fe-III-dipyrido[3,2-a:2',3'-c]phenazine", *J Inorg. Biochem.*, 2009, 103: 1–9. doi:

- 10.1016/j.jinorgbio.2008.08.011
- [7]. Ghosh, K., Tyagi, N., Kumar, P., Singh, U. P., "Synthesis, structure, redox properties and DNA interaction studies on mononuclear iron(III) complexes with amidate ligand", *Inorganica Chim Acta*, 2014, 412: 20–26. doi: 10.1016/j.ica.2013.11.034
- [8]. Chitrapriya, N., Mahalingam, V., Zeller, M., et al., "Synthesis, characterization, DNA binding and cleavage studies of Ru(II) complexes containing oxime ligands", *J. Mol. Struct.*, 2010, 984: 30–38. doi: 10.1016/j.molstruc.2010.09.004
- [9]. Kandaz, M., Yilmaz, I., Keskin, S., Koca, A., "Synthesis, spectroscopy and redox properties of a novel (E-E) vic-dioxime and its mono-, di- and trinuclear complexes bearing an 18-membered N2O2S2 macrocycle", *Polyhedron*, 2002, 21: 0–9. doi: 10.1016/S0277-5387(02)00860-4
- [10]. Dilworth, J. R., Parrott, S. J., "The biomedical chemistry of technetium and rhenium", *Chem. Soc. Rev.*, 1998, 27: 43-55. doi: 10.1039/a827043z
- [11]. Blower, P. J., "Small coordination complexes as radiopharmaceuticals for cancer targeting ", *Transit Met Chem.*, 1998, 23: 109–112. doi: 10.1023/A:1006926505754
- [12]. Vallabhajosula, S., "The Chemistry of Therapeutic Radiopharmaceuticals", *Nuclear Medicine Therapy*, 2012, 339-368. doi: 10.1007/978-1-4614-4021-5_19
- [13]. Ohta, K., Higashi, R., Ikejima, M., et al., "Disk-like liquid crystals of transition metal complexes - Part 21. Critical molecular structure change from columnar to lamellar liquid crystal in bis(diphenylglyoximato)nickel(II)-based complexes ", *J Mater. Chem.*, 1998, 8: 1979–1991. doi: 10.1039/A800897C
- [14]. Nejati, K., Rezvani, Z., Massoumi, B., "Syntheses and investigation of thermal properties of copper complexes with azo-containing Schiff-base dyes", *Dyes and Pigments*, 2007, 75: 653–657. doi: 10.1016/j.dyepig.2006.07.019
- [15]. Karci, F., Ertan, N., "Synthesis of some novel hetarylazo disperse dyes derived from 4-hydroxy-2H-1-benzopyran-2-one (4-hydroxycoumarin) as coupling component and investigation of their absorption spectra", *Dyes and Pigments*, 2005, 64: 243–249. doi: 10.1016/j.dyepig.2004.06.010
- [16]. Tao, T., Xu, F., Chen, X. C., et al., "Comparisons between azo dyes and Schiff bases having the same benzothiazole/phenol skeleton: Syntheses, crystal structures and spectroscopic properties", *Dyes and Pigments*, 2012, 92: 916–922. doi: 10.1016/j.dyepig.2011.09.008
- [17]. EL Mekkawi, D., Abdel-Mottaleb, M. S. A., "The interaction and photostability of some xanthenes and selected azo sensitizing dyes with TiO₂ nanoparticles", *Int. J. Photoenergy*, 2005, 7: 95–101. doi: 10.1155/S1110662X05000140
- [18]. Erdogan, D. A., Özalp-Yaman, Ş., "Novel Pt(II) complexes containing pyrrole oxime, synthesis, characterization and DNA binding studies", *J Mol. Struct.*, 2014, 1064: 50–57. doi: 10.1016/j.molstruc.2014.02.005
- [19]. Chen, G. J., Qiao, X., Qiao, P. Q., et al., "Synthesis, DNA binding, photo-induced DNA cleavage, cytotoxicity and apoptosis studies of copper(II) complexes", *J Inorg. Biochem.*, 2011, 105: 119–126. doi: 10.1016/j.jinorgbio.2010.11.008
- [20]. Suh, J., Chei, W. S., "Metal complexes as artificial proteases: toward catalytic drugs", *Curr. Opin. Chem. Biol.*, 2008, 12: 207–13. doi: 10.1016/j.cbpa.2008.01.028
- [21]. El-Sayed, B. A., Abo Aly, M. M., Emar, A. A., Khalil, S. M. E., "Synthesis and structural study of the ligand o-OH acetophenone azine and its Cu(II), Ni(II), Co(II) and Zn(II) complexes", *Vib. Spectrosc.*, 2002, 30: 93–100. doi: [http://dx.doi.org/10.1016/S0924-2031\(02\)00043-7](http://dx.doi.org/10.1016/S0924-2031(02)00043-7)
- [22]. Baran, T., Karaoğlu, K., Serbest, K., et al., "Studies on synthesis, structure, and DNA cleaving of homo-dinuclear Mn(II), Cu(II), Ni(II), and Zn(II) complexes with a heterocycle-based macrocyclic Schiff base", *Monatshefte für Chemie*, 2013, 144: 1107–1115. doi: 10.1007/s00706-013-0926-6
- [23]. Preti, C., Tassi, L., Tosi, G., et al., "Coordination Chemistry of Cycloserine Derivatives-

- Complexes of Iron(II), Iron(III), Manganese(II) and Palladium(II) with N4-N'4-Tereftal-Bis(Cycloserine)", *J Coord. Chem.*, 1983, 12: 177–185. doi: Doi 10.1080/00958978308073846
- [24]. Geary, W. J., "The use of conductivity measurements in organic solvents for the characterisation of coordination compounds", *Coord. Chem. Rev.*, 1970, 7: 81–122. doi: [http://dx.doi.org/10.1016/S0010-8545\(00\)80009-0](http://dx.doi.org/10.1016/S0010-8545(00)80009-0)
- [25]. Wilson, W. D., Ratmeyer, L., Zhao, M., et al., " The Search for Structure-Specific Nucleic-Acid Interactive Drugs - Effects of Compound Structure on RNA Versus DNA Interaction Strength," *Biochemistry*, 1993, 32: 4098–4104. doi: 10.1021/bi00066a035
- [26]. Li, Y., Wu, Y., Zhao, J., Yang, P.," DNA-binding and cleavage studies of novel binuclear copper(II) complex with 1,1 '-dimethyl-2,2 '-biimidazole ligand ", *Journal of Inorganic Biochemistry*, 2007, 101: 283–290. doi:10.1016/j.jinorgbio.2006.10.004
- [27]. He, X., Jin, L., Tan, L.,"DNA-binding, topoisomerases I and II inhibition and in vitro cytotoxicity of ruthenium(II) polypyridyl complexes: [Ru(dppz)2L]2+ (L = dppz-11-CO2Me and dppz)", *Spectrochim. Acta A Mol. Biomol. Spectrosc.*, 2014, 135: 101–109. doi: 10.1016/j.saa.2014.06.147
- [28]. Janovec, L., Kožurková, M., Sabolová, D., et al., " Cytotoxic 3,6-bis((imidazolidinone) imino)acridines: Synthesis, DNA binding and molecular modeling," *Bioorg. Med. Chem.*, 2011, 19: 1790–1801. doi: 10.1016/j.bmc.2011.01.012
- [29]. Zhu, L.-N., Kong, D.-M., Li, X.-Z., Wang, G.-Y., Wang, J., & Jin, Y.-W., " DNA cleavage activities of tetraazamacrocyclic oxamido nickel(II) complexes ", *Polyhedron*, 2010, 29: 574–580. doi: 10.1016/j.poly.2009.07.021
- [30]. Arjmand, F., Jamsheera, A.," DNA binding studies of new valine derived chiral complexes of tin(IV) and zirconium(IV)", *Spectrochim. Acta - Part A Mol. Biomol. Spectrosc.*, 2011, 78: 45–51. doi: 10.1016/j.saa.2010.06.009
- [31]. Li, D.-D., Tian, J.-L., Gu, W., et al., " A novel 1,2,4-triazole-based copper(II) complex: Synthesis, characterization, magnetic property and nuclease activity ", *J Inorg. Biochem.*, 2010, 104: 171–9. doi: 10.1016/j.jinorgbio.2009.10.020
- [32]. Raman, N., Sobha, S., Mitu, L.," Design, synthesis, DNA binding ability, chemical nuclease activity and antimicrobial evaluation of Cu(II), Co(II), Ni(II) and Zn(II) metal complexes containing tridentate Schiff base ", *J Saudi Chem. Soc.*, 2013, 17: 151–159. doi: 10.1016/j.jscs.2011.03.003
- [33]. Bukhari, S. B., Memon, S., Mahroof-Tahir, M., Bhangar, M. I.,"Synthesis, characterization and antioxidant activity copper-quercetin complex", *Spectrochim. Acta Part A Mol. Biomol. Spectrosc.*, 2009, 71: 1901–1906. doi: 10.1016/j.saa.2008.07.030
- [34]. F. V. Botelho, J. I. Alvarez-Leite, V. S. Lemos, et al., "Physicochemical study of floranol, its copper(II) and iron(III) complexes, and their inhibitory effect on LDL oxidation", *J Inorg. Biochem.*, 2007, 101: 935–943. doi: 10.1016/j.jinorgbio.2007.03.007
- [35]. Wang, Q., Yang, Z.-Y., Qi, G.-F., Qin, D.-D.," Synthesis, crystal structure, antioxidant activities and DNA-binding studies of the Ln(III) complexes with 7-methoxychromone-3-carbaldehyde-(4 '-hydroxy) benzoyl hydrazone ", *Eur. J Med. Chem.*, 2009, 44: 2425–33. doi: 10.1016/j.ejmech.2008.10.023
- [36]. Çol Ayvaz, M., Turan, İ., Dural, B., Demir, S., Karaoğlu, K., Aliyazıcıoğlu, Y., Serbest, K., "Synthesis, in vitro DNA interactions, cytotoxicities, antioxidative activities, and topoisomerase inhibition potentials of Mn(II), Co(II), Ni(II), Cu(II), and Zn(II) complexes with azo-oxime ligands", *Turkish J. Chem.*, 2017, 41: 728–747. doi:10.3906/kim-1612-53.
- [37]. Frisch, M. J., Trucks, G. W., Schlegel, H. B., Scuseria, G. E., et al., *Gaussian 09, revision A.02* Gaussian, Inc, Wallingford, 2009.
- [38]. Becke, A. D., "Density-functional exchange-energy approximation with correct asymptotic behavior", *Phys. Rev. A* 1988, 38: 3098–3100. doi: 10.1103/PhysRevA.38.3098
- [39]. Hariharan, P. C., Pople, J. A.,"The influence of polarization functions on molecular orbital

- hydrogenation energies," *Theor. Chim. Acta* 1973, 28: 213–222. doi: 10.1007/BF00533485
- [40]. Wadt, W. R., Hay, P. J., "Ab initio effective core potentials for molecular calculations. Potentials for the transition metal atoms Sc to Hg", *J Chem. Phys.* 1985, 82: 284–298. doi: 10.1063/1.448800
- [41]. K., Burke, Werschnik, J., Gross, E. K. U., "Time-dependent density functional theory: Past, present, and future", *J Chem. Phys.* 2005, 123: 062206. Doi 10.1063/1.1904586
- [42]. Barone, V., Cossi, M., "Quantum calculation of molecular energies and energy gradients in solution by a conductor solvent model", *J Phys. Chem. A* 1998, 102: 1995–2001. doi: 10.1021/jp9716997
- [43]. N. M. O. Boyle, A. L. Tenderholt, and K. M. Langner, "A library for package-independent computational chemistry algorithms", *J Comput. Chem.* 2008, 29: 839–845. doi: 10.1002/jcc
- [44]. Dennington, T., Millam, R., V. GaussView. J. Semichem Inc. 2009.
- [45]. Cabir, B., Avar, B., Gulcan, M., Kayraldiz, A., Kurtoglu, M., "Synthesis, spectroscopic characterization, and genotoxicity of a new group of azo-oxime metal chelates", *Turkish J Chem.* 2013, 37: 422–438. doi: 10.3906/kim-1210-57
- [46]. Tabassum, S., Sharma, G.C., Arjmand, F., "New modulated design and synthesis of chiral Cu(II)/Sn(IV) bimetallic potential anticancer drug entity: in-vitro DNA binding and pBR322 DNA cleavage activity", *Spectrochim Acta A. Mol Biomol Spectrosc.* 2012, 90, 208-217. doi:10.1016/j.saa.212.01.020
- [47]. Reddy, P. R., Shilpa, A., Raju, N., Raghavaiah, P., "Synthesis, structure, DNA binding and cleavage properties of ternary amino acid Schiff base-phen/bipy Cu(II) complexes", *J Inorg. Biochem.* 2011, 105: 1603–1612. doi: 10.1016/j.jinorgbio.2011.08.022
- [48]. Cheng, C.-C., Rokita, S. E., & Burrows, C. J., "Nickel(III)-Promoted DNA Cleavage with Ambient Dioxide", *Angew. Chem. Int. Ed. Engl.* 1993, 32: 277–278. doi: DOI 10.1002/anie.199302771
- [49]. Lesko, S. A., Lorentzen, R. J., Ts'o, P. O. P., "Involvement of Polycyclic Aromatic-Hydrocarbons and Reduced Oxygen Radicals in Carcinogenesis .5. Role of Superoxide in Deoxyribonucleic-Acid Strand Scission", *Biochemistry* 1980, 19: 3023–3028. doi: Doi 10.1021/Bi00554a029
- [50]. Nilsson, R., Merkel, P. B., Kearns, D. R., "Unambiguous Evidence For The Participation Of Singlet Oxygen ($^1\delta$) In Photodynamic Oxidation Of Amino Acids", *Photochem. Photobiol.* 1972, 16: 117–124. doi: 10.1111/j.1751-1097.1972.tb07343.x
- [51]. Jiang, Q., Xiao, N., Shi, P., et al., "Design of artificial metallonucleases with oxidative mechanism", *Coord. Chem. Rev.* 2007, 251: 1951–1972. doi: 10.1016/j.ccr.2007.02.013
- [52]. A. Turkoglu, M. E. Duru, N. Mercan, et al., "Antioxidant and antimicrobial activities of *Laetiporus sulphureus* (Bull.) Murrill", *Food Chem.* 2006, 101: 267–273. doi: 10.1016/j.foodchem.2006.01.025
- [53]. Hagerman, A. E., Riedl, K. M., Alexander, J., et al., "High molecular weight plant polyphenolics (tannins) as biological antioxidants", *Food Chem.* 1998, 46: 1887–1892. doi: Doi 10.1021/Jf970975b
- [54]. Beauchamp, C., Fridovich, I., "Superoxide dismutase: Improved assays and an assay applicable to acrylamide gels", *Anal. Biochem.* 1971, 44: 276–287. doi: 10.1016/0003-2697(71)90370-8